



島根大学学術情報リポジトリ
S W A N
Shimane University Web Archives of kNowledge

Title

Phosphoric acid and phosphorylation levels are potential biomarkers indicating developmental competence of matured oocytes

Author(s)

Mika Ishigaki, Yumi Hoshino, Yukihiro Ozaki

Journal

Analyst, 2019, Issue5, 144, pp.1527-1534

Published

21 Jan 2019

URL

<https://doi.org/10.1039/C8AN01589A>

この論文は出版社版ではありません。
引用の際には出版社版をご確認のうえご利用ください。

**Phosphoric acid and phosphorylation levels are potential biomarkers
indicating developmental competence of matured oocytes**

Mika Ishigaki^{1,2*}, Yumi Hoshino^{3*}, Yukihiro Ozaki¹

¹School of Science and Technology, Kwansai Gakuin University, 2-1 Gakuen,
Sanda, Hyogo 669-1337, Japan

²Center for Promotion of Project Research, Organization for Research and
Academic Information, Shimane University, 1060 Nishikawatsu-cho,
Matsue, Shimane, 690-8504, Japan

³Graduate School of Biosphere Science, Hiroshima University, 1-4-4
Kagamiyama, Higashi-Hiroshima, Hiroshima, 739-8528, Japan

* Authors to whom correspondence should be sent.

*E-mail: ishigaki-mika@kwansai.ac.jp (M.I.),

hoshimi@hiroshima-u.ac.jp (Y.H.)

Keywords: Raman spectroscopy, Oocyte, Quality evaluation,
Developmental competence, Biomarker

Abstract

Here, we aimed to identify biomarkers for mice oocyte maturation in metaphase II *in vivo* and *in situ* using Raman spectroscopy. Principal component analysis of 324 Raman data points of oocytes at Phase I, II, III, and IV showed that the phosphoric acid concentration uniformly increased in oocytes with higher developmental competence than in oocytes at other maturation stages, and proteins were more phosphorylated. The maturation phases were successfully predicted by linear discriminant analysis with high accuracy (90.7%) using phosphoric molecular information mentioned above. Furthermore, detections of higher concentration of unsaturated fatty acids in overmatured oocytes indicated that a decline in metabolic activity due to overmaturation induced a surplus of these lipid components. Upon assessing invasiveness by laser irradiation, about 50% irradiated oocytes progressed to morula and blastocyst stages in good conditions. Thus, Raman spectroscopy holds promise in evaluating oocyte maturation and quality based on molecular information in infertility treatment.

Introduction

Oocytes are unique and highly specialized cells responsible for creating, activating, and controlling the embryonic genome as well as supporting basic processes, such as cellular homeostasis, metabolism, and cell cycle progression, in the early embryo¹⁻⁴. Oocyte quality is also related to early embryonic survival, establishment and maintenance of pregnancy, fetal development, and adult disease due to mitochondria functional disorder⁵. The biological competence of oocytes is defined as the intrinsic ability to undergo meiotic maturation, fertilization, embryonic development, and successful pregnancy⁶. Developmental competence is gradually acquired during the prolonged process of oogenesis and is essential for optimal development in the final stage, prior to ovulation, because this is when the synchronization between the nuclear and cytoplasmic maturation in oocytes is completed⁶⁻⁹.

In general, oocytes released during ovulation after acquiring developmental competence in metaphase II (MII) are prepared for fertilization. After ovulation, oocytes are overmature and continue aging over time¹⁰. Thus, the optimal period for fertilization with high

developmental competence is limited. Many studies have shown that postovulatory aging leads to limited oocyte competence, abnormal development, congenital malformations, and reduced pregnancy outcomes in mammals¹¹⁻¹⁴.

The developmental competence of oocytes is their ability to undergo successful fertilization, develop into blastocysts, and undergo implantation in the uterus. Many research groups have been investigating to identify markers for selecting the best oocytes and sperm to produce embryos with higher implantation potential¹. In oocytes, the meiotic spindle plays an important role in chromosome alignment and segregation, which are altered considerably during meiotic maturation. Additionally, oocyte morphology, particularly the distance between pericentriolar materials (PCMs), can be used as an indicator during quality evaluation¹⁵. Knowledge on oocyte quality, as reflected by their morphologic and molecular characteristics, is limited due to the lack of availability of MII oocytes for research. Typically, for *in vitro* fertilization (IVF) in the clinical setting, oocyte selection is based on the morphological features of the cytoplasm, polar body, and cumulus cells¹⁶. However, oocyte selection is subjective and controversial and may

not be related to the intrinsic competence of the oocyte¹⁷. In fact, some research groups have focused on studying morphological changes in these oocytes. Nonetheless, the use of oocyte morphology as an indicator of embryo quality remains unreliable¹⁸. Therefore, further studies are needed to elucidate changes in oocytes that better reflect embryo quality in order to establish a clear index.

Raman spectroscopy, one of the vibrational spectroscopies, provides information about vibrational modes of functional groups included in proteins, lipids, and DNA *in situ* without labeling. Especially, strong water bands in the 3800-3200 cm^{-1} do not overlap with Raman bands due to biomolecules mentioned above in the so called fingerprint region^{19,20}. Therefore, Raman spectroscopy is more advantageous to analyze the living cells *in vivo* and *in vitro* than IR and NIR spectroscopies. In recent years, Raman spectroscopy has received much attention for biological and medical applications¹⁹⁻²⁹. Being equipped with a cell incubator, quantitative variations and structural changes of biochemical compositions due to cell division and cell type can be investigated *in vivo*. For example, Notingher evaluated drug toxicity for live cells damaged by an anti-cancer drug

etoposide using Raman spectroscopy²¹. He detected biochemical changes in cells and provided higher discrimination of toxic agents than by other biosensor techniques. Short et al. proved biochemical variations in mammalian cells due to proliferation²². They reported the different variation patterns of proteins, lipids, and RNA between tumorigenic and non-tumorigenic exponential cells. Dochow et al. reported label-free cell type identification using Raman spectroscopy with optical traps and microfluidic environments²³. Furthermore, micro Raman spectroscopy and imaging are beginning to be used for oocyte research²⁴⁻²⁹. Bogliolo et al. investigated oxidative-damage caused by aging in MII oocytes²⁵. They found that young oocytes were clearly distinguished from other damaged groups at the Raman peaks from lipids and proteins. Ishigaki et al. assessed embryonic quality *in situ* by Raman spectroscopy in a nondestructive manner²⁶. They concluded that embryos with low grade morphological features had higher concentrations of lipids, and protein secondary structure changed to α -helix rich forms after fertilization. Heraud et al. achieved 3D molecular Raman imaging of living oocytes²⁷. Wood et al. analyzed the molecular architecture of fixed mouse oocytes²⁸. They revealed the differences between immature

oocytes at the germinal vesicle (GV) stage and mature ones at MII about lipid compositions.

In this study, we investigated the cytoplasmic changes in mouse oocytes over time after ovulation by Raman microscopy and explored the biomarkers characteristic of oocytes having high developmental competence. Raman spectra were obtained from four different stages of oocyte maturation after ovulation. Detailed spectral analysis was performed to clarify the biochemical compositions and structures between oocytes with high and low developmental competence. Moreover, we evaluated the validity of Raman microscopy observations with regard to the quality of oocytes. By comparing the developmental rate of embryos, which progressed to morula or blastocyst stages between oocytes with or without laser irradiation, we proved the near non-invasiveness of Raman measurement in oocytes, although it depends on laser power and experimental conditions. The present results suggest the application of Raman spectroscopy to the non-invasive assessment of oocytes with high developmental competence *in vivo*.

Materials and Methods

Animals

ICR mice were purchased from Japan SLC Inc. (Shizuoka, Japan). Immature 20- to 23-day-old mice were used for all experiments. The experimental procedures described in this report were performed in accordance with the Guide for the Care and Use of Laboratory Animals published by Kwansai Gakuin University.

Oocyte collection

To obtain ovulated oocytes, we first primed the mice with 5 IU pregnant mare's serum gonadotropin (PMSG; Teikoku Hormone MFG, Tokyo, Japan) and then with 5 IU human chorionic gonadotropin (hCG; Teikoku Hormone MFG) after 48 h. Oocytes were collected at 13, 15, 18 and 24 hours after hCG injection, and were subjected to experiments as Phase I, II, III or IV, respectively. Phase I was immediately after the first polar body (PB1) emission, Phase II was the time with the highest developmental competence, and Phase III and IV were the prolonged maturation times after PB1 emission. Distances between PCMs in MII oocytes matured under different conditions were initially long, followed by a gradual shortening, and subsequent

elongation. Fluorescence levels of MTOCs were the highest when the distance between PCMs in MII oocytes was short. The experimental design was set according to the report of Sakai et al. 2011 as shown in Figure 1¹⁵. Solid and dashed lines indicate the incidence rate to MII oocytes and developmental competence, respectively. At each maturation phase, MII-arrested oocytes released from the oviductal ampullae were collected in Leibovitz's L-15 medium (Invitrogen, Grand Island, NY, USA) containing 0.1% polyvinyl alcohol (PVA; Sigma, St. Louis, MO, USA) and 4 mM hypoxanthine (Sigma). The cumulus cells were removed by treatment with 0.1% hyaluronidase at 37 °C.

In vitro fertilization and embryo culture

In vitro fertilization and embryo culture were performed according to previously described methods³⁰. Spermatozoa were collected from the cauda epididymis and pre-incubated for 2 h in 400 µL HTF medium to allow capacitation before insemination. After capacitation, the spermatozoa were introduced into 200-µL droplets of the fertilization medium at a final concentration of 700 spermatozoa/µL. At 4 h after insemination, the

penetration of sperm into the oocytes was confirmed by microscopic examination; subsequently, the oocytes were washed thoroughly five times and then cultured in KSOM medium. All embryos were incubated in 100- μ L droplets of culture medium in a humidified atmosphere of 5% CO₂ in air at 37 °C. The cultured embryos were monitored using a microscope (IX73, OLYMPUS, Japan) with relief contrast, an objective lens with 40 \times magnification (LUCPLFLN 40 \times RC, OLYMPUS, Japan), and a digital camera (DP22, OLYMPUS, Japan).

All experiments were performed in accordance with the fundamental guidelines for the proper conduct of animal experiments and related activities in academic research institutions under the jurisdiction of Ministry of Education, Culture, Sports, Science and Technology in Japan. The present study was approved by the ethics committee of Kwansei Gakuin University and Hiroshima University in Japan.

Raman measurement and Multivariate analysis

The micro Raman system used consisted of a 785-nm diode laser (EXTRA-PS 65, TOPTICA Photonics, Japan), a spectrometer (MCU-301, PHOTO

Design, Japan), a CCD detector (DU401-BR-DD, ANDOR, Japan), and a microscope (IX73, OLYMPUS, Japan) with a 40× immersion type objective lens (UAPON340 40×/1.15, OLYMPUS, Japan). The excitation laser power used was 50 mW at the sample point, and the exposure time was 30 s (2 × 15s). The system was equipped with a CO₂ incubator. During the measurements, oocytes were maintained in L-15 medium including 0.1% PVA at 37 °C.

A Raman spectrum was obtained at 1–3 points per oocyte for each maturation phase. The numbers of oocytes used for measurement at each maturation phase were 47 (I), 43 (II), 48 (III), and 35(IV), respectively. The Raman spectra measured were calibrated using the peak series of indene. The background due to the Raman system, quartz dish, and culture media was subtracted from the original spectra, and autofluorescence background of the sample was removed using 5th-order polynomial fitting. The spectral intensity was normalized with a standard peak at 1004 cm⁻¹ from phenylalanine. Averaged Raman spectra for each developmental stage were calculated using preprocessed Raman data. Multivariate analyses such as principal component analysis (PCA) and linear discriminant analysis (LDA)

were performed with chemometrics software Unscrambler X 10.1 (CAMO, Japan). PCA method extracts a set of orthogonal principal components (PCs) to account for the maximum variance in the spectral dataset. An original spectrum can be reproduced by summing up all PC components multiplied of loadings and scores. LDA was performed using the score vectors of PCA^{31,32}. The Raman spectral dataset for LDA included all maturation stages. LDA model was developed using the half data selected at random, and the remaining half data was validated by applying the model.

Results and Discussion

Raman Spectra of Mouse Oocytes at Four Maturation Stages

Raman spectra obtained from oocytes at four different maturation stages were compared. Figure 2 shows averaged Raman spectra in the 1800–600 cm^{-1} region of mouse oocytes obtained at Phases I (n=105), II (n=88), III (n=96), and IV (n=35) after the injection of hCG hormone. Many notable bands from proteins, lipids, and DNA/RNA were clearly observed. A peak at 1004 cm^{-1} is due to the ring breathing of phenylalanine³³⁻³⁵, and its peak height was used as an internal standard for the normalization of Raman

spectra. A doublet at 853 and 830 cm^{-1} comes from Fermi resonance between a ring breathing mode and the overtone of an out-of-plane ring bending vibration of tyrosine³³⁻³⁵. Bands at 1084 and 1048 cm^{-1} are due to the symmetric stretching vibration of PO_4^{3-} , and the one at 1084 cm^{-1} originates from symmetric phosphate backbone vibration of PO_2^- in DNA³⁶⁻³⁸. A broad feature around 1266 cm^{-1} contains overlapping bands due to the ring breathing modes of DNA/RNA (T, A), amide III, and bending mode of =C-H of lipids. A band at 1451 cm^{-1} arises from C-H deformation modes of lipids, proteins, and carbohydrates, and the one at 1309 cm^{-1} is due to CH_3/CH_2 twisting and bending modes. A band at 1656 cm^{-1} is the overlap of two bands assigned to Amide I modes of proteins and the C=C stretching modes of lipids³³⁻³⁵. The detailed assignment of prominent Raman bands is shown in Table 1.

In order for qualitative analysis to extract the different molecular components depending on the maturation time after ovulation, PCA was performed on the data set of 324 Raman spectra of oocytes including all maturation phases. The score plots using principal component (PC) 1 and PC4 of PCA exhibits a good separation pattern of each maturation phase as

shown in Figure 3a, and these PCs show characteristic components of oocytes for each maturation phase. Figure 3b illustrates the loading plots of PC1 and PC4. Figure 3a shows that the dataset was roughly classified into two groups about the PC1 axis: the centroids of Phase I, II, and III score plots exist in minus for the x-axis with some variations, and Phase IV on the other hand, is on the plus side for the x-axis. Figure 3c shows the averages of PC1 scores for each maturation stage and Phase IV clearly shows a positive value. PC1 loading shows some characteristic peaks at 1064, 1080, 1120, 1271, 1308, 1445, 1658, and 1742 cm^{-1} due to lipids, and their assignments are given in Table 2^{33-35,39}. These results indicate that Phase IV oocytes have high concentrations of lipids compared to oocytes at other maturation stages. Moreover, the PC1 loading plot appears like a Raman spectrum of unsaturated fatty acids³⁹. Furthermore, the former (Phase I and II) and the latter (Phase III and IV) stages seem to be grouped by the PC4 component (Figure 3a). The loading plot of PC4 shows a striking peak at 1046 cm^{-1} due to the PO_4^{3-} symmetric stretching vibration^{37,38}. Figure 3d demonstrates the averages of PC4 scores for each maturation phase, and they show different signs between the former and the latter phases. This indicates that the

concentration of phosphoric acid is higher in the former phase than in the latter phase. Actually, the peak intensities at 1046 cm^{-1} in averaged Raman spectra were higher and lower in the former (I: 0.65, II: 0.63) and the latter (III: 0.56, IV: 0.56) phases, respectively. Furthermore, phosphoric acid is assumed to have a specific conformation indicated by the peaks at 1080 and 980 cm^{-1} . The ratio of these peak intensities ($980/1080\text{ cm}^{-1}$) in averaged Raman spectra had also higher and lower values in the former (I: 0.87, II: 0.94) and the latter (III: 0.84, IV: 0.77) phases, respectively. The detailed discussion about its conformation is mentioned in the next section.

Molecular Key Factors for Fertility and Viability of Oocytes

It was found that oocytes in Phase II with high fertility and viability had high concentrations of phosphoric acids, and the ones with extremely these low abilities on Phase IV had increased lipid components¹⁵. Phosphoric acids and lipids were indicated as possible key factors to discriminate fertility and viability competence of oocytes. First, it is well known that lipid components are one of the most potent energy sources for embryonic development⁴⁰⁻⁴², and they should be appropriately metabolized for the proper growth of

oocytes. In general, culture conditions *in vivo* are the best for oocytes⁴³. Sakai et al. proved that mouse oocytes cultured *in vivo* had a higher rate of development to the blastocyst stage, compared to oocytes cultured *in vitro*¹⁵. Furthermore, it has been reported that embryos with abnormal metabolism incubated *in vitro* had a higher lipid concentration than the ones *in vivo*⁴⁴. The evaluation of embryonic quality using Raman spectroscopy by Ishigaki et al. also showed that mouse embryos with lower-grade morphological features had a higher concentration of lipids than the ones with high-grade features²⁶. From their perspective of the relationship between lipid metabolism and embryonic survival potential, the embryonic conditions with a higher lipid concentration, as indicated by the present Raman study, can be interpreted as a metabolic abnormality by the loss of their viability competence. Therefore, it can be assumed that the metabolic activity decreased and lipid components failed to be properly metabolized on Phase IV.

Phosphoric acid is indicated as a key factor to characterize oocyte maturation by PCA. Maturation promoting factor (MPF) is a cytoplasmic factor to control the transition of eukaryotic cells into M-phase^{45,46}. MPF is

a specific protein kinase in M-phase, and it plays important roles in the mammalian oocyte meiosis. MPF is composed of two proteins, namely histone kinase p34 (cdc2) and cyclin B, and it phosphorylates proteins to make them functional in the regulation of cell division⁴⁶. The activation of MPF is controlled by the phosphorylation of cdc2; only MPF phosphorylated at T161, of the three phosphorylation sites (T14, Y15, and T161), becomes active^{35,48}. It has been well known that the concentration of activated MPF increases in the first and second meiotic stages⁴⁷; MPF controls these meiotic divisions⁴⁵. Oocytes measured in the present study were on the second meiotic metaphase. They stop their second meiotic division and wait to restart it by fertilization with maintaining MPF activation⁴⁹. However, MPF activity cannot be retained for a long time, and decreases with overmaturation⁴⁹. Therefore, MPF activity is expected to increase in the early phase (I and II) and generally proteins are more phosphorylated by activated MPF.

In the loading plot of PC4 (Figure 3b), other peaks at 1080 and 980 cm^{-1} due to phosphoric acids with opposite directions are assigned to monobasic ($-\text{OPO}_3\text{H}^-$) and dibasic ($-\text{OPO}_3^{2-}$) phosphate stretching vibration,

respectively^{50,51}. It is well known that phosphate groups exist as fully protonated structures ($-\text{OPO}_3\text{H}_2-$) under strong acid conditions ($\text{pH} < 2$), and as dibasic under basic conditions ($\text{pH} > 10$)^{50,51}. Dibasic and monobasic forms coexist between these conditions including biological pH, and the relative contribution of each depends on pH. The more active the life activity, the more ATP is produced by mitochondria and the higher the phosphoric acid concentration. It has been reported that the decrease in mitochondria-derived ATP levels causes a decay of the spindle fine structure⁵². Moreover, results showing that the meiotic spindle has a fine structure in phase II¹⁵ may be supported by a higher concentration of ATP. It is natural to conclude that a higher concentration of phosphoric acid can maintain MPF activity, and a higher activation of MPF can more effectively phosphorylate proteins.

Modification of proteins with phosphoric acids alters the protein conformation, activity, and function. In eukaryotic cells, side chains of three amino acids, namely serine, threonine, and tryptophan, are phosphorylated⁵³. Kinases that phosphorylate serine or threonine control meiotic divisions^{54,55}, and tyrosine kinases play an important role in oocyte maturation and fertilization^{56,57}. Raman intensity due to monobasic phosphate at 1080 cm^{-1}

decreased and that due to dibasic phosphate at 980 cm^{-1} increased in the pH range of 5~7 by phosphorylation of serine and threonine^{50,51}. That is, the fact that the peaks at 1080 and 980 cm^{-1} appeared downward and upward in the PC4 loading, respectively, can be interpreted as proteins being more phosphorylated in the earlier phase (I and II) than in the latter one. In this way, it has been widely recognized that the phosphorylation of MPF and three amino acids is important for oocyte maturation and meiotic division. However, protein phosphorylation has to be investigated one by one for each protein using conventional, destructive methods such as ELISA (Enzyme-Linked Immunosorbent Assay)^{58,59}. Even though it is difficult to discriminate the species of phosphorylated proteins based on Raman results, the present method provided a comprehensive overview of all protein and kinase phosphorylation in oocytes. That is, activation of biomolecules by phosphorylation could be detected nondestructively.

Linear Discriminant Analysis of Maturation Phases by PCA-LDA

In order to evaluate the possibility of discrimination of maturation stages based on molecular information, especially according to phosphoric acid and

phosphorylation levels, PCA-LDA was performed. The total number of Raman spectra including all maturation stages was 324 (13 h: 105, 15 h: 88, 18 h: 96, 24 h: 35). To develop an LDA model, half the data points (162) were used and reliability of the model was validated by using the remaining 162 data points. The model was built based on PC4 scores, which captured the slight component differences of maturation stages, to separate the early phase (I and II) and the latter (III and IV). The zero value of the LDA score was the border to separate between the early and the latter phases. The data assigned to the positive LDA score were identified as the early phase and the ones with a negative value as the latter. The LDA score plot is shown in Figure 4. The maturation stages were correctly predicted in all phases with 84.5% accuracy. The detailed list of sample number for all maturation stages and prediction rate are shown in Table 3. In the early phase, Phase I data were classified into the early phase with 80.8% accuracy, but their LDA score had a wide range of values from high to low. The result indicates that the concentrations of phosphoric acid and phosphorylation are not uniform for each site and each oocyte. At Phase II, on the other hand, prediction rate of the stage was 90.7% and positive LDA scores were observed. In the latter

phase, the scores reduced to negative values. The 79.2% prediction rate at Phase III implied that 20.8% oocytes still had good phosphoric conditions, but they could no longer uniformly maintain it. In the end, Phase IV data were correctly discriminated as the latter phase with 94.4% accuracy. Table 4 summarizes the results showing the relationship between developmental competence, homogeneity of phosphorylation level, concentration of phosphoric acid and lipid contents. Judging comprehensively from these results, oocytes in Phase II uniformly showed the highest potential for fertility and viability.

The advantage of the present LDA analysis is that it was prepared using the data set obtained by point mode measurements. Recently, some reports about biochemical composition and the local dependency of their variations in mouse oocytes using Raman mapping have been published²⁷⁻²⁹. It is true that oocytes have local dependency on biochemical compositions, and a Raman imaging technique in more dimensions is attractive. However, Raman measurements in plane or cube may cause more harmful phototoxicity for oocytes due to longer laser exposure, and its application to the assessment of oocyte quality seems to be difficult given the current

technology. However, the fact that our present results showed extremely high prediction values of fertility and viability competences based on molecular compositions even though the analyzed data set included local and individual dependencies shows great promise for the oocyte quality assessment.

Evaluation of laser invasiveness

The laser invasiveness for oocytes was evaluated. Oocytes after Raman measurement were fertilized *in vitro* and incubated for five days. The measurement condition was the same as already mentioned above. Laser was exposure limited to Raman measurement and laser irradiation was restricted to one point per an oocyte. In order to evaluate the effect caused by laser irradiation, non-irradiated oocytes were also incubated as controls. Figure 5 demonstrates visible images of incubated embryos on the fifth day; (a) laser irradiated and (b) non-irradiated embryos. Several blastocysts and morula can be seen and some of them already hatched in both Figure 5(a) and (b). Figure 5(c) exhibits the developmental rates (%) of oocytes that progressed to morula or blastocyst stages after fertilization. The developmental rates of irradiated (n =97) and non-irradiated (n =17) oocytes amounted to 51.5%

and 82.4%, respectively. By comparing these results, a slight descent of the developmental rate of irradiated oocytes can be seen compared to the control. Other data of cultivation with the same ovulation treatment showed a 13.4~60.7% developmental rate¹⁵; thus, it can be concluded that almost no effect of laser irradiation was observed.

The significance of the evaluation for laser irradiation to oocytes was to prove that embryogenesis progressed after laser irradiation. Before the experiment, we had expected that embryos would hardly develop because the laser power was set high to get Raman spectra with a high signal to noise ratio for the analysis to extract the biochemical differences. It is possible to decrease the total energy of laser irradiation by adjusting the laser power and irradiation time. The present results show the possibility to establish completely non-invasive and safe conditions of Raman measurement of oocytes. The results proving the non-invasive effect of laser irradiation to oocytes provide useful information for practical application to the assessment of the embryonic development and quality using Raman spectroscopy.

Conclusion

In the present study, we identified key molecular factors determining oocyte maturation *in vivo* using Raman spectroscopy. Oocytes, at maturation Phase II (15 h) with higher developmental competence, showed a higher concentration of phosphoric acid and more phosphorylated sites on proteins than those of older maturation phases III and IV. Furthermore, these phosphoric states were maintained without showing individual or local dependencies. Using spectral parameters including concentration of phosphoric acids and protein phosphorylation to discriminate maturation phases by LDA, Phase II data were correctly classified as the early phase (I and II) with 90.7% accuracy. The present Raman data obtained by point mode measurements intrinsically included individual and local dependencies. It was a remarkable finding that one can evaluate maturation oocyte with high accuracy in spite of these ambiguities. Moreover, metabolic abnormality due to overmaturation was likely to induce a higher concentration of fatty acids in Phase IV because these components were not properly metabolized. Furthermore, it was surprising that laser irradiated oocytes showed a high rate of development to morula and blastocyst stages

contrary to the original expectation. The results indicated near non-invasiveness of Raman measurement. This is a great advance to exhibit a possible new non-invasive method to evaluate developmental competence based on molecular composition in actual infertility treatments.

Conflicts of interest

There are no conflicts to declare.

Acknowledgements

This work was supported by JSPS KAKENHI Grant Number 17K18267 (M.I.) and 26712022 (Y.H.). We thank Prof. Hidetoshi Sato in Kwansai Gakuin University for our usage of microscope Raman system.

References

1. G. Ruvolo et al. *J. Assist. Reprod. Genet.* 2013, **30**, 207-212.
2. G. Coticchio et al. *Hum. Reprod. Update*, 2015, **21(4)**, 427-454.
3. P. May-Panloup et al. *Hum. Reprod. Update*, 2016, **22(6)**, 725-743.
4. B. P. Mihalas et al. *Oxid. Med. Cell. Longe.*, 2017, 4015874, 22.
5. M. R. Chiaratti, et al. *Cell Biol. Int.*, 2018, **42**, 711-724.
6. J. J. Eppig et al. *Dev. Biol.*, 1994, **164(1)**, 1-9.
7. M. G. Da Broi et al. *J. Assist. Reprod. Genet.*, 2018, **35(5)**, 735-751.
8. S. M. Downs. *Reprod. Fertil. Dev.*, 2015, **27(4)**, 572-582.
9. R. B. Gilchrist et al. *Reproduction*, 2016, **152(5)**, R143-R157.
10. Y. L. Miao et al. *Hum. Reprod. Update*, 2009, **15(5)**, 573-585.
11. T. Trapphoff et al. *Hum. Reprod.*, 2016, **31**, 133-149.
12. R. H. Hunter. *Mol. Reprod. Dev.*, 1991, **29**, 385-391.
13. T. Takahashi et al. *J. Obstet. Gynaecol. Res.*, 2013, **39(10)**, 1431-1439.
14. S. Prasad et al. *J. Biomed. Sci.*, 2015, **22(1)**, 36.
15. C. Sakai et al. *J. Assist. Reprod. Genet.*, 2011, **28(2)**, 157-166.
16. G. Coticchio et al. *Ann. N. Y. Acad. Sci.*, 2004, **1034(1)**, 132-144.
17. P. F. Serhal et al. *Hum. Reprod.*, 1997, **12(6)**, 1267-70.

18. A. M. Sanchez et al. *J. Ovarian. Res.*, 2017, **10(1)**, 43.
19. Y. Ozaki. *Appl. Spectrosc. Rev.*, 1998, **24(3-4)**, 259-312.
20. P. Carey. *Biochemical applications of Raman and resonance Raman spectroscopies*. Elsevier, New York, 2012.
21. I. Notingher. *Sensors*, 2007, **7(8)**, 1343-1358.
22. K. W. Short et al. *Biophys. J.*, 2005, **88(6)**, 4274-4288.
23. S. Dochow et al. *Lab Chip*, 2011, **11(8)**, 1484-1490.
24. W. E. Huang et al. *Anal. Chem.*, 2004, **76(15)**, 4452-4458.
25. L. Bogliolo et al. *J. Assist. Reprod. Genet.*, 2013, **30(7)**, 877-882.
26. M. Ishigaki et al. *Sci. Rep.*, 2017, **7**, 43942.
27. P. Heraud et al. *Sci. Rep.*, 2017, **7**, 8945.
28. B. R. Wood et al. *Anal. Chem.*, 2008, **80(23)**, 9065-9072.
29. B. Davidson et al. *J. Raman Spectrosc.*, 2012, **43(1)**, 24-31.
30. Y. Hoshino and E. Sato. *Dev. Biol.*, 2008, **314**, 215-223.
31. W. Zhao et al. *Discriminant analysis of principal components for face recognition*. H. Wechsler et al. (eds) *Face Recognition*, Springer, Berlin, Heidelberg, 1998, pp. 73-85.
32. Y. Tominaga. *Intell. Lab.*, 1999, **49**, 105-115.

33. Z. Movasaghi, S. Rehman and I. U. Rehman. *Appl. Spectrosc. Rev.*, 2007, **42(5)**, 493-541.
34. I. Notingher et al. *Anal. Chem.*, 2004, **76(11)**, 3185-3193.
35. N. Stone et al. *Faraday Discuss.*, 2004, **126**, 141-157.
36. W. T. Cheng et al. *Microsc. Res. Tech.*, 2005, **68(2)**, 75-79.
37. G. Penel et al. *Calcif. Tissue Int.*, 1998, **63(6)**, 475-481.
38. I. Notingher et al. *J. Royal Soc. Interface*, 2004, **1(1)**, 79-90.
39. J. R. Beattie et al. *Lipids*, 2006, **41(3)**, 287-294.
40. T. Watanabe et al. *BMC Cell Biol.*, 2010, **11(1)**, 38.
41. K. R. Dunning et al. *Biol. Reprod.*, 2010, **83(6)**, 909-918.
42. P. Haggarty et al. *Hum. Reprod.*, 2006, **21(3)**, 766-773.
43. P. Holm and H. Callesen. *Reprod. Nutr. Dev.*, 1998, **38(6)**, 579-594.
44. M. Barcelo-Fimbres and G. E. Seidel. *Mol. Reprod. Dev.*, 2007, **74(11)**, 1406-1418.
45. J. Gerhart, M. Wu and M. Kirschner. *J. Cell Biol.*, 1984, **98(4)**, 1247-1255.
46. I. Hoffmann et al. *EMBO J.*, 1993, **12(1)**, 53-63.
47. B. Ducommun et al. *EMBO J.*, 1991, **10(11)**, 3311-3319.

48. M. J. Solomon, T. Lee and M. W. Kirschner. *Mol. Biol. Cell*, 1992, **3(1)**, 13-27.
49. S. Brunet and B. Maro. *Reproduction*, 2005, **130(6)**, 801-811.
50. L. Ashton, C. Johannessen and R. Goodacre. *Anal. Chem.*, 2011, **83(20)**, 7978-7983.
51. Y. Xie, Y. Jiang and D. Ben-Amotz. *Anal. Biochem.*, 2005, **343(2)**, 223-230.
52. X. Zhang et al. *Cell Res.*, 2006, **16(10)**, 841.
53. A. Kreegipuu, N. Blom and S. Brunak. *Nucleic Acids Res.*, 1999, **27(1)**, 237-239.
54. M. Conti et al. *Mol. Cell. Endocrinol.*, 2012, **356(1-2)**, 65-73.
55. J. Liu and J. L. Maller. *Curr. Biol.*, 2005, **15(16)**, 1458-1468.
56. K. I. Sato, A. A. Tokmakov and Y. Fukami. *Comp. Biochem. Physiol. B: Biochem. Mol. Bio.*, 2000, **126(2)**, 129-148.
57. W. H. Kinsey. *Biochem. Biophys. Res. Commun.*, 1997, **240(3)**, 519-522.
58. Y. Y. Hu et al. *The Am. J. Pathol.*, 2002, **160(4)**, 1269-1278.
59. E. Vanmechelen et al. *Neurosci. Lett.*, 2000, **285(1)**, 49-52.

Table 1: Peak assignment of averaged Raman spectra.

Peak (cm ⁻¹)	DNA/RNA	proteins	lipids	carbohydrates	others
830	asym str PO ₂ ⁻	ring br Tyr			
853		ring br Tyr			
935		C-C BK str			
1004		sym ring br Phe			
1033		Phe			
1048					sym str PO ₄ ³⁻
1084	sym str PO ₂ ⁻	C-N str			sym str PO ₄ ³⁻
1129		C-N str		C-O str	
1250-1275	T, A	Amide III	=C-H ben		
1309		CH ₃ /CH ₂ twi, ben	CH ₃ /CH ₂ twi, ben		
1451		CH def	CH def	CH def	
1656		Amide I	C=C str		

Table 2: Assignment of characteristic peaks in loading plot of PC1.

Peak (cm ⁻¹)	Assignment
1064	C-C, C-O stretching
1080	C-C, C-O stretching
1120	C-C stretching
1271	=C-H bending
1308	CH ₃ /CH ₂ twisting, bending
1445	CH ₃ /CH ₂ bending, deformation
1658	C=C, C=O stretching
1742	C=O stretching

Table 3: List of samples for all maturation stages and prediction rate (P.R.)

validated by PCA-LDA.

		True stage			
		I, II		III, IV	
		13h	15h	18h	24h
Prediction	I, II	42	39	10	1
	III, IV	10	4	38	17
	P.R. (%)	80.8	90.7	79.2	94.4

Table 4: Summary of the results showing the relationship between developmental competence, homogeneity of phosphorylation level, concentration of phosphoric acid, and lipid content.

	Phase I	Phase II	Phase III	Phase IV
Developmental competence	Not high	High	Not high	Low
Homogeneity of oocyte	-	+	-	-
Phosphoric acid content	+++	++	-	-
Lipid	-	-	-	+++

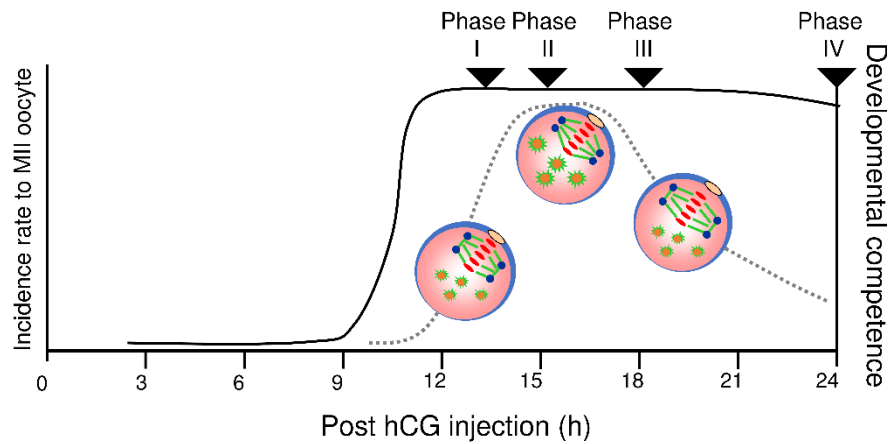


Figure 1: Experimental design. In this experiment, oocytes were collected at 13, 15, 18 and 24 hours after hCG injection, and were subjected to experiments as Phase I, II, III or IV, respectively. Solid and dashed lines indicate incidence rate to MII oocyte and developmental competence, respectively. This experimental design was set according to the report of Sakai et al. 2011.

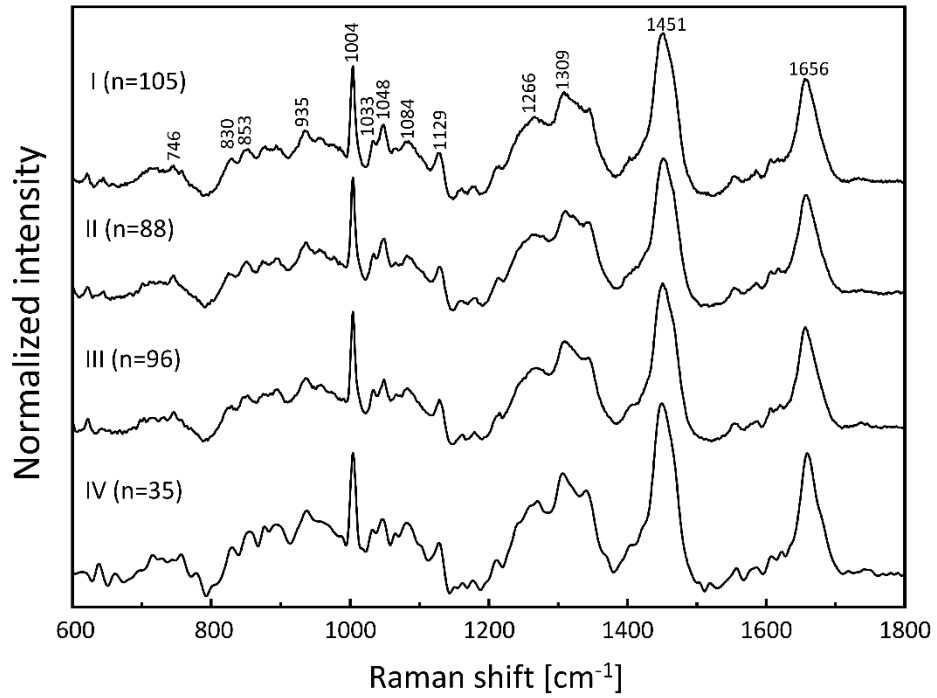
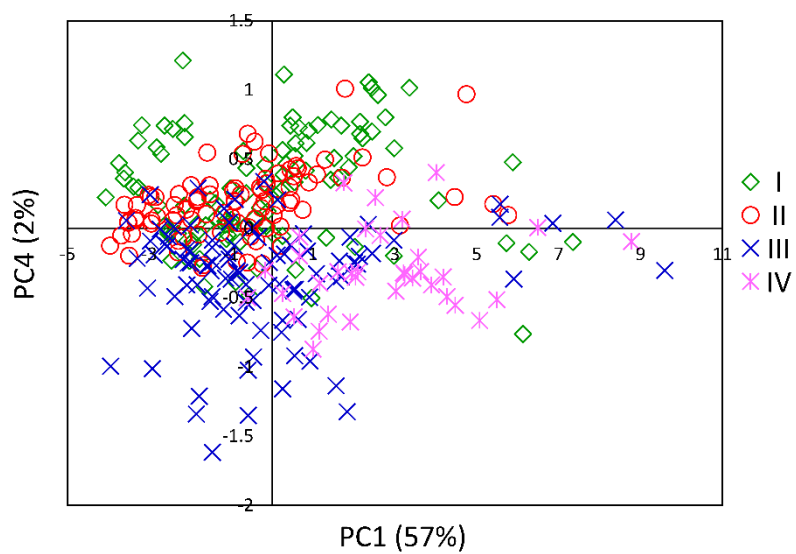
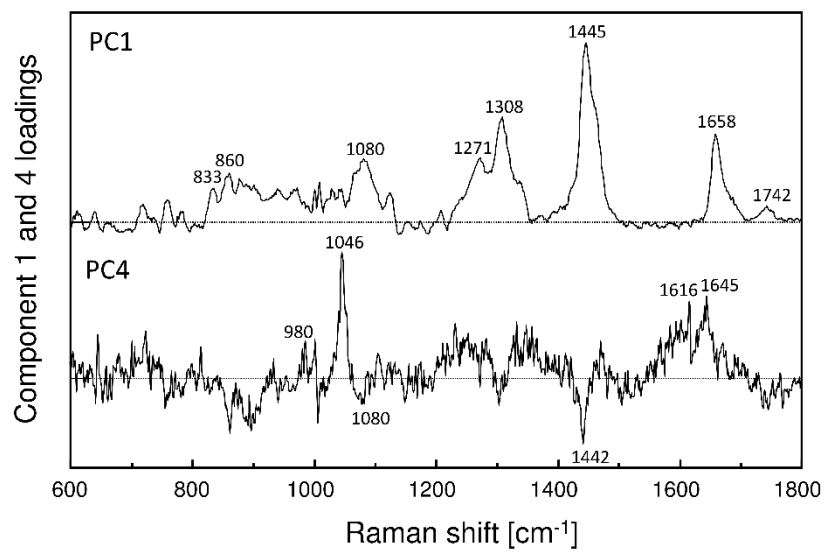


Figure 2: The averaged Raman spectra in the 1800-600 cm^{-1} region of mouse embryos obtained from Phase I (n=105), II (n=88), III (n=96), and IV (n=35) after injection of hCG hormone.

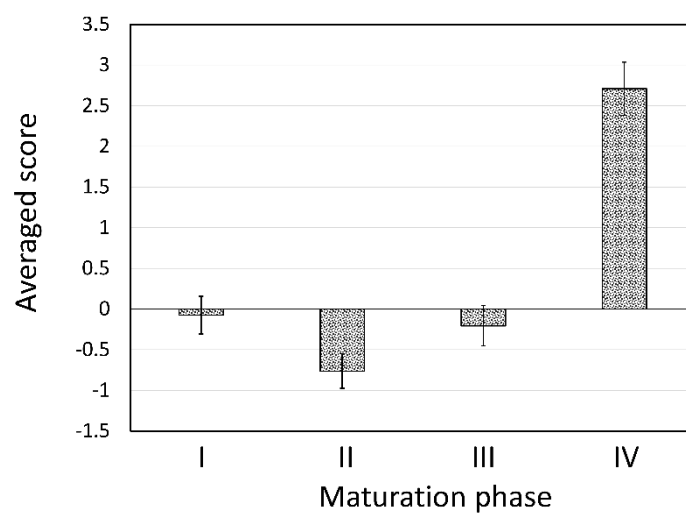
(a)



(b)



(c)



(d)

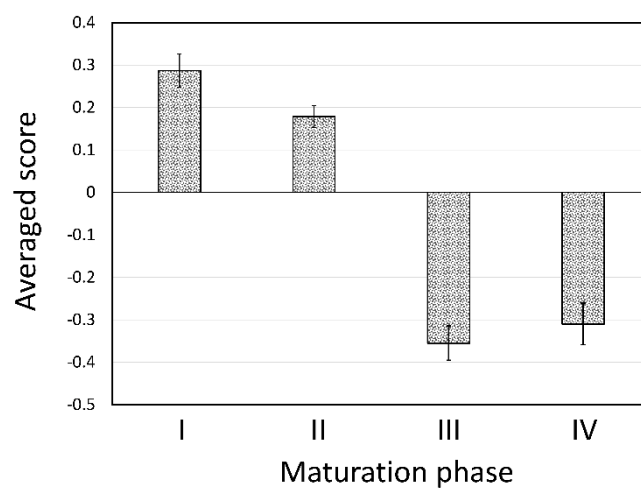


Figure 3: (a) Score plots of PC1 and PC4 of PCA performed on the data set including 324 Raman spectra of mouse oocytes in all maturation stages. (b) Loading plots of PC1 and PC4 of PCA in (a). (c) and (d) are averaged scores of PC1 and PC4 in (a), respectively, with the standard error.

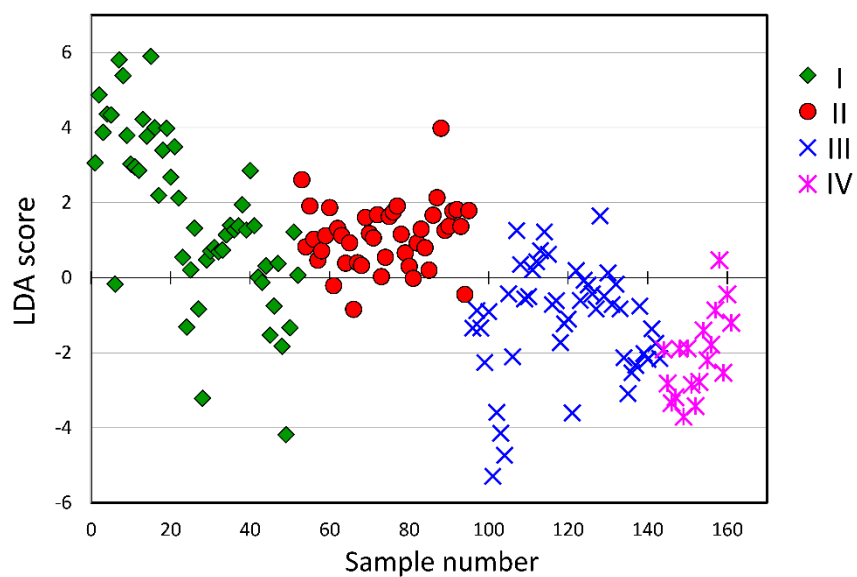


Figure 4: Score plot of LDA validation. 162 samples Raman spectral data were used to build an LDA model and the remaining 162 samples were validated by the model. The zero value of the LDA score is the border to separate between the early (I and II) and latter (III and IV) phases.

(a)



(b)



(c)

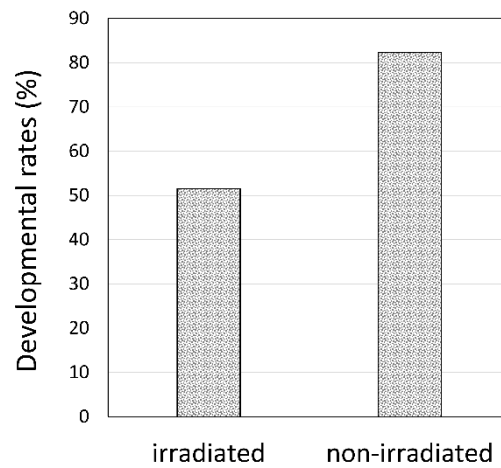


Figure 5: Visible image of embryos incubated for five days; (a) laser irradiated and (b) non-irradiated embryos. Several blastocysts and morula can be seen and some of them already hatched in both (a) and (b). (c) Developmental rates (%) of oocytes after fertilization that progressed to morula or blastocyst stages.